ACS OMEGA

http://pubs.acs.org/journal/acsodf

Article

TEMPO-Cellulose Nanocrystal-Capped Gold Nanoparticles for Colorimetric Detection of Pathogenic DNA

Keya Ganguly, Dinesh K. Patel, Sayan Deb Dutta, and Ki-Taek Lim*

Cite This: *ACS Omega* 2021, 6, 12424–12431

Read Online

ACCESS | Metrics & More | Article Recommendations | Supporting Information

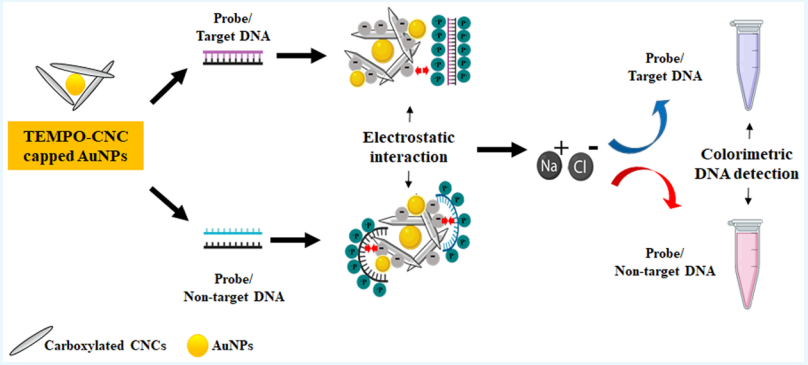

ABSTRACT: Nanocellulose-assisted gold nanoparticles are considered promising materials for developing eco-friendly diagnostic tools for biosensing applications. In this study, we synthesized 2,2,6,6-tetramethylpiperidin-1-piperidinyloxy (TEMPO)-oxidized cellulose nanocrystal (TEMPO-CNC)-capped gold nanoparticles (AuNPs) for the colorimetric detection of unamplified pathogenic DNA oligomers of methicillin-resistant *Staphylococcus aureus*. The fabricated TEMPO-CNC-AuNPs (TC-AuNPs) were characterized using UV−visible spectroscopy, transmission electron microscopy, atomic force microscopy, and dynamic light scattering. The average diameter of the synthesized AuNPs was approximately 30 nm. The aqueous solution of TC-AuNPs was stable and exhibited an absorption peak at 520 nm. The chemical interaction between TC-AuNPs and the surface charge of the target and non-target DNA determined the colorimetric differences under ionic conditions. A dramatic color change (red → blue) was observed in the TC-AuNP solution with the target DNA under ionic conditions due to the aggregation of AuNPs. However, no observable color change occurred in the TC-AuNP solution with the non-target DNA under similar conditions owing to the better shielding effects of the charged moieties. The colorimetric detection limit of the TC-AuNPs was demonstrated to be as low as 20 fM pathogenic DNA. Therefore, the use of TEMPO-oxidized CNC-capped AuNPs is efficient and straightforward as a biosensor for the colorimetric detection of pathogenic DNA.

1. INTRODUCTION

Gold nanoparticle (AuNP)-based colorimetric biosensors have emerged as a robust diagnostic toolkit in medicine[1,2] due to their unique characteristics, including a high aspect ratio, specific spectral absorption, and ability to bind to DNA and proteins.[3] The salt-induced surface plasmon resonance (SPR) spectral properties of AuNPs have been widely studied for the detection of single- and double-stranded DNA molecules.[4] The stabilization or/and destabilization of the nucleotide-nanoparticle complexes under ionic conditions is profoundly affected by the interaction between DNA-AuNPs.[5] Based on AuNP aggregation, numerous point-of-care nanobiosensors have been developed over the years.[6]

The detection of pathogenic infection by AuNP-based biosensors has received significant interest for their application in wound healing with respect to skin patches.[7] These patches often induce pathogenic cell lysis and leakage.[8] Quick on-site identification of the genetic material of novel pathogens at the site of skin infection can help us to choose an appropriate medication.[9] The sensing of pathogenic nucleic acids by biosensors has enormous beneficial applications. The AuNP-based colorimetric detection of nucleic acids can be implemented for such applications in conjugation with biocompatible capping agents with tunable chemical properties.

Carbohydrate-coated AuNPs have been adopted to support green chemistry-based diagnostic approaches. The glyco-AuNPs are highly stable, biocompatible, easy to synthesize,

Received: January 20, 2021
Accepted: March 11, 2021
Published: March 22, 2021

and exhibit a notable detection limit for target molecules.[10−12] The dextrin-coated AuNPs were synthesized for the colorimetric detection of the unamplified DNA of *Pseudomonas cubensis* up to a limit of 2.94 fM.[4] Dextrin-capped AuNPs have also been used for the electrochemical detection of the *IS16110* gene from *Mycobacterium tuberculosis* up to 0.01 ng/μL of concentration.[13] Glucose-AuNPs also have wide theranostic applications.[14] Therefore, glyco-AuNPs have great potential for DNA detection, even in complex biological environments.

Cellulose nanocrystals (CNCs) have several advantages over their neutral polysaccharide macro-analog for use as capping and stabilizing agents because of their unique properties such as high stiffness, low density, well-defined size, specific morphology, controlled and tunable surface chemistry, environmental sustainability, and anticipated low cost.[15] CNC properties can be easily tuned through surface functionalization.[16] Improved metal adsorption properties were observed in the carboxylated CNCs.[17] The 2,2,6,6-tetramethylpiperidin-1-piperidinyloxy (TEMPO) oxidation process is frequently applied to generate the carboxylated TEMPO-CNCs (TC).[18]

In this study, we synthesized and evaluated the potential application of TC-stabilized AuNPs for the colorimetric detection of pathogenic DNA. We used pathogenic DNA from MRSA for the colorimetric detection due to their pathogenicity. We successfully detected the target pathogenic DNA oligomer up to 20 fM within 2−3 min. The schematic presentation for the colorimetric detection of the target and non-target pathogenic DNA in the presence of TC- stabilized AuNPs under ionic conditions is shown in Figure 1.

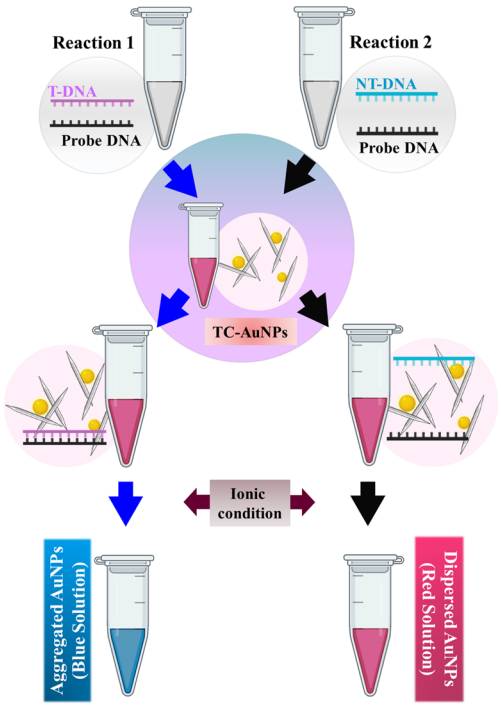

Figure 1. Schematic illustration of the colorimetric detection of methicillin-resistant *Staphylococcus aureus* (MRSA) DNA using TEMPO-CNC-stabilized AuNPs (TC-AuNPs). T-DNA: target DNA, NT-DNA: non-target DNA, TC-AuNPs: TEMPO-CNC-capped AuNPs.

2. RESULTS AND DISCUSSION

2.1. Characterizations of TC-AuNPs. The UV−visible spectra of the TC and TC-AuNP solutions are shown in Figure 2a. No absorption peak was observed in the TC solution, whereas the TC-AuNP solution exhibited an absorption peak at 520 nm, indicating the presence of AuNPs. The redox reaction between $HAuCl_4$ and NaOH resulted in the generation of AuNP, indicated by the change in color from yellow to red. The synthesized TC-AuNP solution was homogenous and stable. Images of the TC and TC-AuNP solutions are given in the inset of Figure 2a.

The surface charge, hydrodynamic radius, and polydispersity index (PDI) of the TC and TC-AuNP solutions are given in Table 1 and were −36.9 ± 10.4 mV, 107.4 ± 57.86 nm, and 0.20 ± 4.7, respectively, for TC and −43.4 ± 7.5 mV, 1841 ± 7.0 nm, and 0.51 ± 0.9, respectively, for the TC-AuNP solution. These enhancements in the surface charge and hydrodynamic radius were due to the attachment of TC to the AuNPs. The increased PDI indicates the polydispersity characteristic of the synthesized TC-AuNPs.[19]

The ultrahigh resolution-transmission electron microscopic (UHR-TEM) image of the synthesized AuNPs is shown in Figure 2b. The size of the synthesized AuNPs was approximately 30 nm, and they were well dispersed in the media. TC was distributed around the generated TC-AuNPs. The distribution of TC around the formed AuNPs is responsible for the high hydrodynamic radius, as observed in the DLS measurements. The solution pH plays a significant role in the dispersion of the nanomaterial. The surface charge of TC and the pH 7.0 of the medium facilitated the well-dispersed and homogenous solution of the formed AuNPs.[20] The AFM image of TC-AuNPs is presented in Figure 2c. The average size of the synthesized nanoparticles was approximately 40 nm. A schematic demonstration of the synthesis of TC-AuNPs is shown in Figure S1.

2.2. Salt-Induced Aggregation of TC-AuNPs with or without ssDNA Probe. The aggregation tendency of nanoparticles under ionic environments plays a crucial role in the colorimetric detection of the target biomolecule.[21,22] A high degree of dispersion under an ionic environment indicates greater stability of the nanoparticles.[23] The UV−visible spectra of the synthesized TC-AuNPs in the presence of different concentrations (0 → 10 mM) of NaCl solution are shown in Figure 3a. The pure TC-AuNPs exhibited an absorption peak at 520 nm, which shifted toward a higher wavelength with an increase in the concentration of the NaCl solution in the media. This red shift was due to the increase in the electronic conjugation between the nanoparticles, leading to the aggregation of the TC-AuNPs.[24] Hoeng et al. reported the effects of the surface charge density of carboxylated CNCs on the stability of synthesized silver nanoparticles (AgNPs), observing that the charge density is an important factor in the stability of AgNPs.[25] The colorimetric change in the TC-AuNP solution in the presence of different concentrations of NaCl solution is given in the inset of Figure 3a. No significant color change was observed in the NaCl solution up to a concentration of 5 mM, indicating this as the stability limit of the TC-AuNPs. However, a change in color (red → blue) was observed in the NaCl solution at a concentration greater than 5 mM. This change in color was due to the salt-induced aggregation of the TC-AuNPs, causing the red shift in the spectra. The colorimetric changes of the TC-AuNP solution in

https://doi.org/10.1021/acsomega.1c00359
ACS Omega 2021, 6, 12424−12431

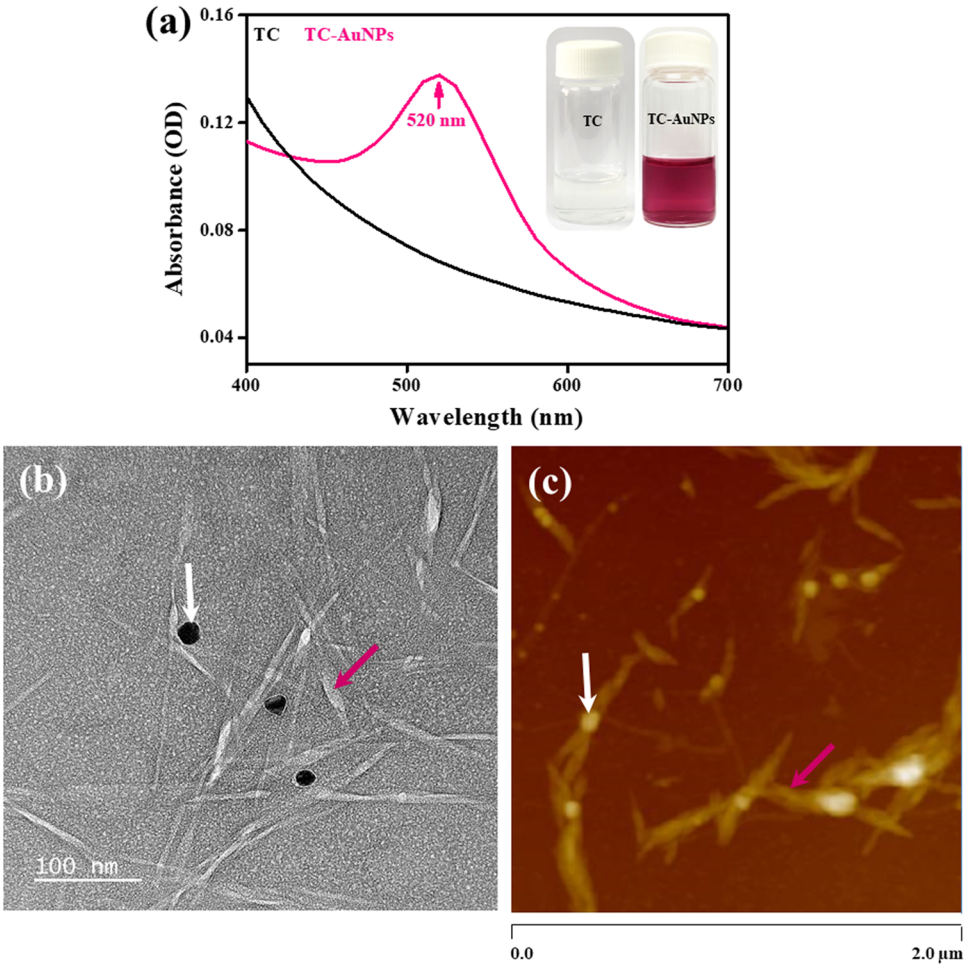

Figure 2. Chemical and morphological characterization of the synthesized TEMPO-CNC-AuNPs (TC-AuNPs). (a) UV−vis spectrum with the corresponding digital photograph of TC and TC-AuNPs; (b) UHR-TEM morphology of TC-AuNPs dispersed in water; (c) AFM morphology of TC-AuNPs dispersed in water; white arrows and red arrows indicate the AuNPs and TC.

Table 1. Physicochemical Characterization of the AuNPs[a]

sample	ζ-potential (mV)	average size (nm)	polydispersity index (PDI)
TC	−36.9 ± 10.4	107.4 ± 57.86	0.20 ± 4.70
TC-AuNPs	−43.4 ± 7.5	1841 ± 7.0	0.59 ± 0.9

[a]Zeta potential values, mean particle size, and polydispersity index (PDI) of the samples.

the presence of different concentrations of NaCl solution at 0 times are shown in Figure S2a,b. No significant visible color change was observed for the TC-AuNP solution at 0 time. The changes in the ratio of UV−vis absorbance at 620 (SPR of aggregated AuNPs) and 520 nm (SPR of dispersed AuNPs) denoted as A620/A520 of TC-AuNPs and ssDNA-incorporated TC-AuNPs in the presence of different concentrations (0 → 10 mM) of NaCl solution are shown in Figure 3b. No significant changes in the absorbance values were observed up to 5 mM NaCl solution in both TC-AuNP and ssDNA-incorporated TC-AuNP media, indicating their stability limit. However, more significant changes in this value occurred in the TC-AuNP media compared with the ssDNA-incorporated TC-AuNP media at NaCl concentrations higher than 5 mM, showing a lower aggregation tendency of the TC-AuNPs in the presence of the ssDNA probe, due to the shielding effects of the ssDNA probe. The electronic environment of the ssDNA probe acts as a barrier and prevents the aggregation of TC-AuNPs in the presence of ionic conditions. The colorimetric changes of the TC-AuNP and ssDNA-incorporated TC-AuNP media in the presence of different concentrations of NaCl solution are shown in the inset of Figure 3b. The TC-AuNP solution exhibited a color change after adding 3 mM NaCl. In contrast, no such color change was observed in the ssDNA-incorporated TC-AuNP solution up to 5 mM NaCl, demonstrating their better stability.

The A620/A520 values for varying concentrations of ssDNA-incorporated TC-AuNPs in the presence of 6 mM NaCl are presented in Figure 3c. Here, we chose 6 mM NaCl to monitor the colorimetric changes in ssDNA-incorporated TC-AuNP media due to the effectiveness of NaCl at this concentration. A decrease in the A620/A520 value was observed by increasing the ssDNA probe concentrations in the solution, indicating the better shielding effects of the ssDNA probe. The colorimetric changes at varying concentrations of the ssDNA-incorporated TC-AuNP solution in the presence of 6 mM NaCl are shown in the inset of Figure 3c. Resistance to color change (red → blue) occurred at a higher concentration of ssDNA, showing the stability of TC-AuNPs due to the enhanced barrier effects of the probe.

2.3. Colorimetric Detection of Pathogenic DNA. The UV−visible absorption spectra of TC-AuNPs with or without

https://doi.org/10.1021/acsomega.1c00359
ACS Omega 2021, 6, 12424−12431

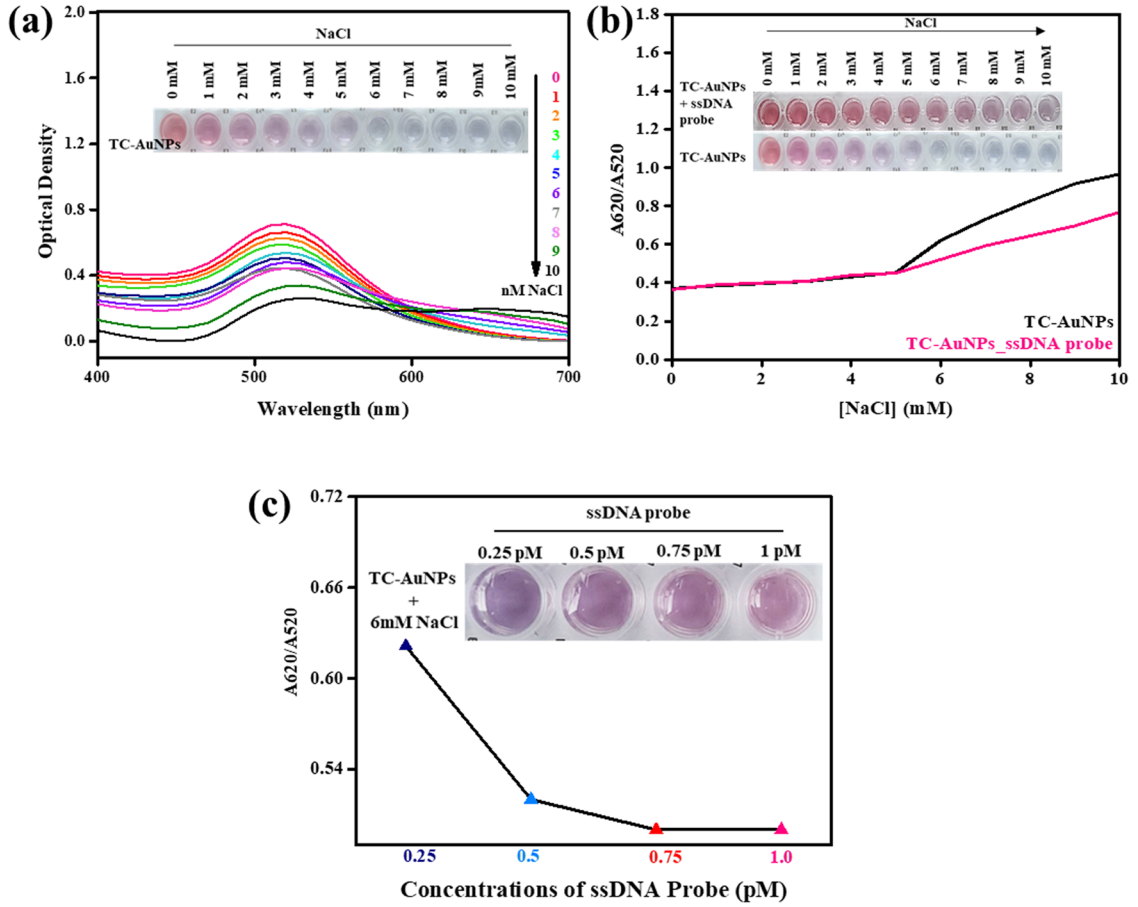

Figure 3. Aggregation pattern of TC-AuNPs. (a) With increasing NaCl concentrations, (b) in the presence of the 0.25pM ssDNA probe and the A620/A520 ratio in the presence of the ssDNA probe, and (c) in the presence of increasing concentration of the ssDNA probe with a corresponding A620/A520 ratio.

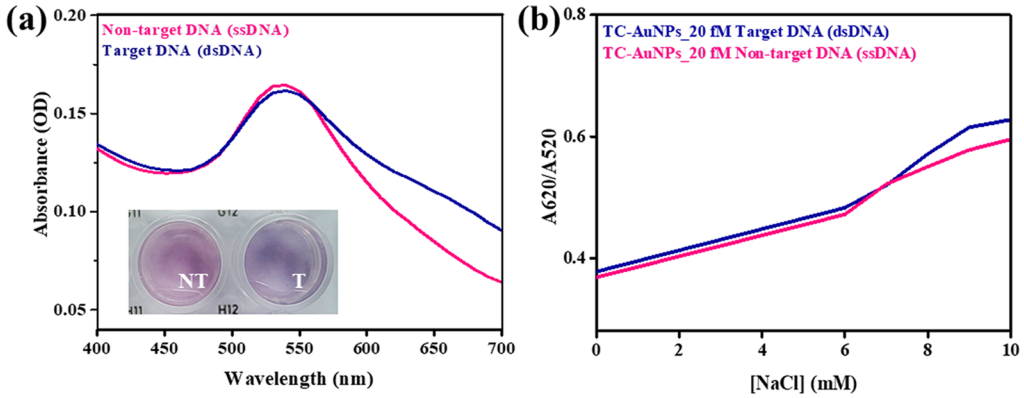

Figure 4. Spectral and colorimetric detection of pathogenic DNA. (a) Spectral and corresponding colorimetric changes in the presence of 20 fM non-target and target DNA. (b) Aggregation pattern of the TC-AuNPs with increasing salt concentration, 20 fM dsDNA, and 20 fM ssDNA.

the target DNA (20 fM) in the presence of 8 mM NaCl solution are shown in Figure 4a. The target media exhibited an absorption peak at 535 nm, which shifted toward a higher wavelength (540 nm) in the non-target media, indicating the aggregation of the TC-AuNPs. This shift in the wavelength was due to the low shielding effects of the probe DNA in the target conditions, causing agglomeration. This agglomeration leads to electronic conjugation and facilitates red shifting in the UV−visible spectra. The colorimetric changes of the TC-AuNPs with or without the target DNA in the presence of 8 mM NaCl solution are presented in the inset of Figure 4a. A significant color change (red → blue) was observed in the target media due to the agglomeration of TC-AuNPs. In comparison, no such color change occurred in the non-target media. The electrostatic interaction between ds/ssDNA and TC-AuNPs is responsible for the color change in the media.[26] The changes in the A620/A520 values of TC-AuNPs with or without the target DNA (20 fM) were assessed using a spectrophotometer, and the results are shown in Figure 4b. Interestingly, the target DNA exhibited a higher value than the non-target DNA, indicating an aggregation of the TC-AuNPs. This is attributed to the poor shielding effects of the hybridized ssDNA probe

https://doi.org/10.1021/acsomega.1c00359
ACS Omega 2021, 6, 12424−12431

and the complementary target in the target media under ionic conditions. The hybridization of the ssDNA probe with the target and non-target pathogenic DNA at different periods was monitored by gel electrophoresis, and the results are shown in Figure S3. The target DNA was hybridized with the ssDNA probe and exhibited greater intensity than the unhybridized non-target DNA.

2.4. UHR-TEM Analysis of TC-AuNPs with or without Pathogenic DNA. The agglomeration behavior of the ssDNA-incorporated TC-AuNPs with or without target DNA (20 fM) in the presence of 8 mM NaCl solution was evaluated by UHR-TEM, and the results are shown in Figure 5a,b. The non-target media showed the well-dispersed nature of the TC-AuNPs. However, agglomeration of the TC-AuNPs was observed in the target media. The UHR-TEM images clearly show the dispersed and agglomerated TC-AuNPs in non-target and target media, causing color changes, respectively. This result indicated that NaCl destabilized the TC-AuNPs in the presence of dsDNA, while the ssDNA stabilized the AuNPs.

We proposed a schematic model for the interaction mechanism between the TC-AuNPs and DNA under ionic conditions based on the obtained results, and the model is shown in Figure 6. The destabilization of the synthesized TC-AuNPs occurred in the presence of NaCl. The salt-induced aggregation of TC-AuNPs was prevented by ssDNA in a dose-dependent manner. However, no shielding effect was observed in the presence of dsDNA, causing the aggregation of TC-AuNPs. This difference indicates the effect of DNA conformation as a controlling factor in the colorimetric changes of TC-AuNPs. For ssDNA, it is believed that the negatively charged phosphate groups of the DNA are distanced from the TC-AuNPs by the electrostatic repulsion between the negatively charged CNCs and phosphates, while the nitrogen bases are oriented toward the charged CNCs through attraction, leading to the formation of a protective layer. This layer acts as a barrier for NaCl and prevents the destabilization of TC-AuNPs. In the case of dsDNA, all nitrogen bases are bound to their respective units. Therefore, no electrostatic attraction occurred between the nitrogen bases of the dsDNA and charged CNCs, which restricted the formation of the protective layer around the TC-AuNPs, and NaCl easily destabilized it, leading to agglomeration and, consequently, color change. Additionally, the developed TC-AuNPs showed good biocompatibility, as shown in Figure S4. A comparative list of different polysaccharide-mediated AuNPs for the colorimetric detection of pathogenic DNA or target molecules, with their respective detection limits, is given in Table 2. We emphasize that the synthesized TC-AuNPs have a promising potential for the detection of biomolecules owing to the unique properties of the nanocellulose and AuNPs.

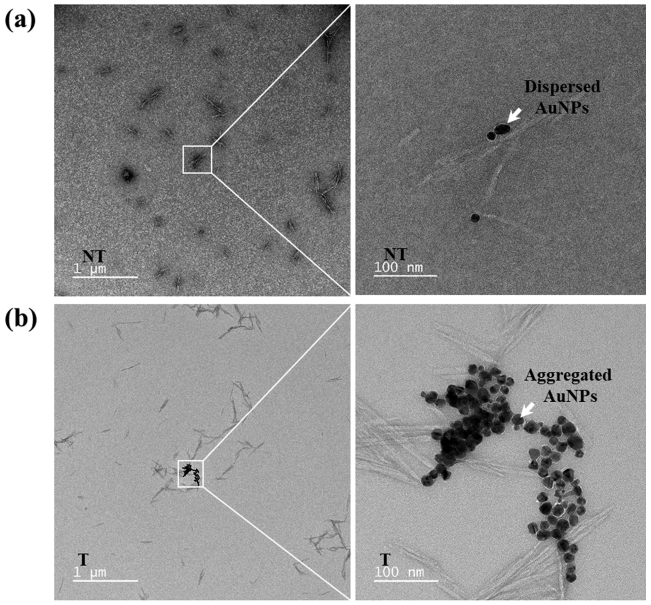

Figure 5. UHR-TEM images of the TC-AuNPs in the presence of (a) non-target and (b) target DNA.

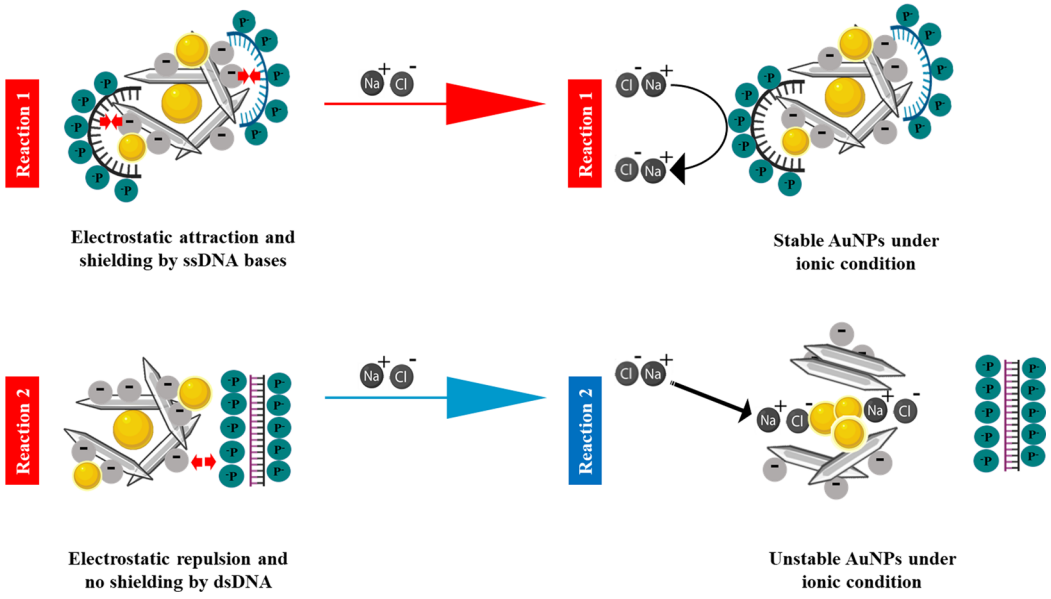

Figure 6. Illustration of the proposed mechanism of the interaction of non-target (upper panel) and target DNA (lower panel) with TEMPO-CNC-stabilized AuNPs (TC-AuNPs) under ionic conditions for the sequence-specific detection of pathogenic DNA.

https://doi.org/10.1021/acsomega.1c00359
ACS Omega 2021, 6, 12424−12431

Table 2. Comparison of the Synthesized TC-AuNP-Based Sensing Performance with Other Reported Glyco-Capped AuNP-Mediated Target Detection

carbohydrate-capped nanoparticles	target	minimum detection limit/time	detection method	references
TC-AuNPs	methicillin-resistant *S. aureus* (MRSA ssDNA)	20 fM/3 min	spectral and colorimetric	present work
glycan/AuNPs	viral receptor		fluorescence quenching	27
sucrose/AuNPs	Zika virus in*Ae. aegypti* salivary protein	1.0×10^5 PFU live Zika virus	spectral and colorimetric	28
sucrose/AuNPs	ciprofloxacin	12 $\mu g\ L^{-1}$ 15.8 $\mu g\ L^{-1}$	colorimetric	29
mannose/BSA/Au nanocluster	concanavalin A	0.62 nM	fluorescence	30
dextran/AuNPs	*Pseudoperonospora cubensis* DNA	2.9 fM/30 min	spectral and colorimetric	4
dextran/AuNPs	dengue-1 virus	0.01 μM/20 min	colorimetric lateral flow	31
chitosan/AuNPs	*M. tuberculosis* DNA	0.342 mg/mL of chitosan	colorimetric	32
chitosan/AuNPs	cimetidine	3 ng mL^{-1}/2 min	spectral and colorimetric	33

3. CONCLUSIONS

The properties of the developed AuNP-based biosensors are widely influenced by the capping material used in the synthesis process. Therefore, the selection of a suitable capping agent with superior tunable properties is required to improve the detection properties of the synthesized AuNPs. For this, CNCs are considered an ideal material owing to their superior and tunable physicochemical properties. A homogenous and stable solution of AuNPs was obtained in the presence of carboxylated functionalized CNCs. It is interesting to note that the stability of the synthesized AuNPs increased in the presence of the ssDNA probe under ionic conditions due to the formation of a protective layer. A change in color (red → blue) was observed in the target media under ionic conditions due to an agglomeration of the TC-AuNPs, as observed in the TEM image. However, no color change occurred in the non-target media. The stabilization and destabilization of the TC-AuNPs under ionic conditions are responsible for the change in the color of the media. The color change can be easily visualized within 3 min in the target media with a detection limit of 20 fM concentration of the pathogenic DNA.

Our approach provides an eco-friendly, cost-effective, biocompatible, and rapid detection system based on the surface charge densities of the interacting particles. We believe that the developed material shows great potential for its application as a biosensor for the colorimetric detection of pathogenic DNA and warrants further research in this direction.

4. EXPERIMENTAL SECTION

4.1. Materials. Gold(III) chloride trihydrate ($HAuCl_4 \cdot 3H_2O$, 99.9% trace metal basis), agarose, and sodium chloride (NaCl) were purchased from Sigma-Aldrich (USA) and were used without further purification. TEMPO-CNCs were received from the Cellulose Lab (Canada) and used as obtained. Sodium hydroxide (NaOH) was purchased from JUNSEI (Japan). The ssDNA probe and target and non-target DNA were received from BIONEER Inc. (Daejeon, Republic of Korea). Dulbecco's modified Eagle's medium (DMEM), 10% fetal bovine serum (FBS), and antibiotics Penicillin–Streptomycin (P/S) were purchased from Welgene Inc. (Republic of Korea). A WST-1 dye (EZ-Cytox cell viability assay kit) was purchased from DoGenBio Co., Ltd. (Seoul, Republic of Korea).

4.2. Synthesis of TC-AuNPs. The synthesis of TC-AuNPs was performed, as previously reported elsewhere with some modifications.[34] Briefly, the stock solution (50 mL) of 1 mM $HAuCl_4$ was prepared in an aqueous medium and heated up to 90 °C with vigorous stirring (MSH-30D, DAIHAN Scientific, Republic of Korea) under dark conditions followed by the addition of 500 μL of TEMPO-CNC solution. The pH ∼7 of the mixture solution was adjusted by incorporating the required amounts of 1 M NaOH solution. The change in the color (yellow → red) indicated the completion of the reaction.

4.3. Characterization of TC-AuNPs. A spectrophotometer (Softmax Pro Molecular Device, Version 7, California) was used to measure the absorbance of TC and TC-AuNPs in the range of 400−700 nm. The morphology of the TC-AuNPs was monitored by ultrahigh resolution transmission electron microscopy (UHR-TEM; AARM 1300S, Jeol, Japan) with a resolution of 0.12 nm and atomic force microscopy (AFM) (Nanoscope 5 Bruker, USA). The dynamic light scattering (DLS) and zeta potential (ζ) values of TC-CNCs and TC-AuNPs were measured using a particle size analyzer (Malvern Panalytical, UK; Zetasizer Ver 7.13).

4.4. Assay Procedure. The stability of the synthesized TC-AuNPs was evaluated in the presence of the different concentrations of NaCl (0, 1, 2, 3, 4, 5, 6, 7, 8, 9, and 10 mM) at room temperature, and the absorption spectra of the solution were measured by a spectrophotometer. The effect of ssDNA on the aggregation pattern of the TC-AuNPs in the presence of similar concentrations of NaCl was evaluated by incubating the TC-AuNPs with a 0.25 pM ssDNA probe for 10 min at RT followed by the addition of NaCl, as described before. The absorption spectrum was recorded after 10 min of incubation at RT. To study the effect of increasing concentration of ssDNA in the aggregation pattern of TC-AuNPs, we had incubated the nanoparticles with 0.25, 0.5, 0.75, and 1 pM ssDNA for 10 min followed by NaCl treatment for the next 10 min. The absorption spectrum was recorded at 620 and 520 nm wavelengths.

4.5. Detection of Unamplified *S. aureus* ssDNA. The target and the non-target DNA oligomers dissolved in ultrapure water were incubated with an equal amount of the ssDNA probe at RT for 15 min to allow hybridization followed by the addition of 5 μL of the incubated DNA into 105 μL of TC-AuNPs. The mixture solution was further incubated at RT for 10 min. The NaCl solution (8 mM) was gradually added into the mixture solution till the color change.

The DNA sequences used in this study are listed in Table 3.

4.6. Determination of DNA Hybridization. The hybridization of the probe with the target and the non-target DNA was analyzed by 2% agarose gel electrophoresis. The gel images

https://doi.org/10.1021/acsomega.1c00359
ACS Omega 2021, 6, 12424−12431

Table 3. List of DNA Sequences Used in this Study

sample	sequences
ssDNA probe	5′-ATG ATT ATG GCT CAG GTA CTG CTA TCC ACC-3′
target DNA	5′-GGT GGA TAG CAG TAC CTG AGC CAT AAT CAT-3′
non-target DNA	5′-GCG AGA TGA TTA TGG CTC AGG TAC TGC TAT-3′

were captured using a molecular imager (Molecular Imager Chemi Doc XRS+ Imaging System).

4.7. Cell Viability Assay. The human bone marrow-derived mesenchymal stem cells (hBMSCs) were obtained from KCLB, Seoul National University (Republic of Korea) and maintained in DMEM supplemented with 10% FBS and 1% P/S. The cell viability of hBMSCs in the presence of TC-AuNPs (0.25, 0.5, 1, and 2 μM) was analyzed using the WST-1 assay followed by incubation for 1, 3, and 5 days. The cell viability was recorded by measuring the absorbance at 450 nm. hBMSCs without TC-AuNPs served as the control set. All the samples were prepared in triplicate, and data were presented as mean ODs ± standard deviations.

4.8. Statistical Analysis. Statistical analysis was carried out using Origin Pro 9.0 software (OriginLab, Massachusetts, USA). Statistical significance between the control and treatment group was determined using one-way analysis of variance (ANOVA). All the data were presented as mean ± SDs of triplicate experiments. Differences were considered significantly at $*p < 0.05$.

■ ASSOCIATED CONTENT

Supporting Information

The Supporting Information is available free of charge at https://pubs.acs.org/doi/10.1021/acsomega.1c00359.

Schematic illustration of the synthesis of TC-AuNPs (Figure S1), the aggregation pattern of TC-AuNPs at 0 s (Figure S2), agarose gel electrophoresis of hybridized DNA after indicated time intervals (Figure S3), and cytotoxicity evaluation of hBMSCs in the presence of TC-AuNPs (Figure S4) (PDF)

■ AUTHOR INFORMATION

Corresponding Author

Ki-Taek Lim − *Department of Biosystems Engineering, Institute of Forest Science, Kangwon National University, Chuncheon 24341, Republic of Korea;* orcid.org/0000-0003-2091-788X; Email: ktlim@kangwon.ac.kr

Authors

Keya Ganguly − *Department of Biosystems Engineering, Institute of Forest Science, Kangwon National University, Chuncheon 24341, Republic of Korea*

Dinesh K. Patel − *Department of Biosystems Engineering, Institute of Forest Science, Kangwon National University, Chuncheon 24341, Republic of Korea*

Sayan Deb Dutta − *Department of Biosystems Engineering, Institute of Forest Science, Kangwon National University, Chuncheon 24341, Republic of Korea*

Complete contact information is available at: https://pubs.acs.org/10.1021/acsomega.1c00359

Notes

The authors declare no competing financial interest.

■ ACKNOWLEDGMENTS

This research was supported by the "Basic Science Research Program" through the "National Research Foundation of Korea" (NRF) funded by the "Ministry of Education" (NRF-2018R1A6A1A03025582 and 2019R1D1A3A03103828). We would like to thank the Korea Basic Science Institute (KBSI), Chuncheon for providing the TEM facility and Kangwon National University Central Laboratory for providing the AFM facility.

■ REFERENCES

(1) Xing, Y.; Zhu, Q.; Zhou, X.; Qi, P. A gold nanoparticle-based colorimetric mercury(II) biosensor using a DNA probe with phosphorothioate RNA modification and exonuclease III-assisted signal amplification. *Microchim. Acta* **2020**, *187*, 214−218.

(2) Nguyen, Q. H.; Kim, M. I. Nanomaterial-mediated paper-based biosensors for colorimetric pathogen detection. *TrAC, Trends Anal. Chem.* **2020**, *132*, 116038.

(3) Bai, X.; Wang, Y.; Song, Z.; Feng, Y.; Chen, Y.; Zhang, D.; Feng, L. The Basic Properties of Gold Nanoparticles and their Applications in Tumor Diagnosis and Treatment. *Int. J. Mol. Sci.* **2020**, *21*, 2480.

(4) Baetsen-Young, A. M.; Vasher, M.; Matta, L. L.; Colgan, P.; Alocilja, E. C.; Day, B. Direct colorimetric detection of unamplified pathogen DNA by dextrin-capped gold nanoparticles. *Biosens. Bioelectron.* **2018**, *101*, 29−36.

(5) Zhang, Q.; Zou, X.-N.; Chu, L.-Q. Surface plasmon resonance studies of the hybridization behavior of DNA-modified gold nanoparticles with surface-attached DNA probes. *Plasmonics* **2018**, *13*, 903−913.

(6) Alizadeh, S.; Nazari, Z. A Review on Gold Nanoparticles Aggregation and Its Applications. *J. Chem. Rev.* **2020**, *2*, 228−242.

(7) Juknius, T.; Juknienė, I.; Tamulevičius, T.; Ružauskas, M.; Pamparienė, I.; Oberauskas, V.; Jurkevičiūtė, A.; Vasiliauskas, A.; Tamulevičius, S. Preclinical study of a multi-layered antimicrobial patch based on thin nanocomposite amorphous diamond like carbon films with embedded silver nanoparticles. *Materials* **2020**, *13*, 3180.

(8) Jamaledin, R.; Yiu, C. K. Y.; Zare, E. N.; Niu, L.-N.; Vecchione, R.; Chen, G.; Gu, Z.; Tay, F. R.; Makvandi, P. Advances in antimicrobial microneedle patches for combating infections. *Adv. Mater.* **2020**, *32*, 2002129.

(9) Lloyd-Smith, J. O.; Funk, S.; McLean, A. R.; Riley, S.; Wood, J. L. N. Nine challenges in modelling the emergence of novel pathogens. *Epidemics* **2015**, *10*, 35−39.

(10) Adokoh, C. K.; Keter, F. K.; Kinfe, H. H.; Tshikhudo, R.; Darkwa, J. Development and characterization of functionalized glyco thiolate capped gold nanoparticles for biological applications. *RSC Med. Chem.* **2020**, *11*, 283−292.

(11) Kveton, F.; Blsakova, A.; Kasak, P.; Tkac, J. Glycan Nanobiosensors. *Nanomaterials* **2020**, *10*, 1406.

(12) Sun, J.; Lu, Y.; He, L.; Pang, J.; Yang, F.; Liu, Y. Colorimetric sensor array based on gold nanoparticles: Design principles and recent advances. *TrAC, Trends Anal. Chem.* **2020**, *122*, 115754.

(13) Torres-Chavolla, E.; Alocilja, E. C. Nanoparticle based DNA biosensor for tuberculosis detection using thermophilic helicase-dependent isothermal amplification. *Biosens. Bioelectron.* **2011**, *26*, 4614−4618.

(14) Suvarna, S.; Das, U.; Kc, S.; Mishra, S.; Sudarshan, M.; Saha, K. D.; Dey, S.; Chakraborty, A.; Narayana, Y. Synthesis of a novel glucose capped gold nanoparticle as a better theranostic candidate. *PLoS One* **2017**, *12*, No. e0178202.

(15) Aziz, T.; Fan, H.; Zhang, X.; Haq, F.; Ullah, A.; Ullah, R.; Khan, F. U.; Iqbal, M. Advance Study of Cellulose Nanocrystals Properties and Applications. *J. Polym. Environ.* **2020**, *28*, 1117−1128.

(16) Rincón-Iglesias, M.; Lizundia, E.; Correia, D. M.; Costa, C. M.; Lanceros-Méndez, S. The role of CNC surface modification on the structural, thermal and electrical properties of poly (vinylidene fluoride) nanocomposites. *Cellulose* **2020**, *27*, 3821−3834.
(17) Karim, Z.; Hakalahti, M.; Tammelin, T.; Mathew, A. P. In situ TEMPO surface functionalization of nanocellulose membranes for enhanced adsorption of metal ions from aqueous medium. *RSC Adv.* **2017**, *7*, 5232−5241.
(18) Isogai, A.; Zhou, Y. Diverse nanocelluloses prepared from TEMPO-oxidized wood cellulose fibers: Nanonetworks, nanofibers, and nanocrystals. *Curr. Opin. Solid State Mater. Sci.* **2019**, *23*, 101−106.
(19) Mudalige, T.; Qu, H.; Van Haute, D.; Ansar, S. M.; Paredes, A.; Ingle, T. Characterization of Nanomaterials: Tools and Challenges. In *Nanomaterials for Food Applications*; Amparo, L. R.; Maria, J. F. R.; Marta, M. S.; Laura, G. G.-M. Ed.; Elsevier, 2019, pp. 313−353.
(20) Ganguly, K.; Patel, D. K.; Dutta, S. D.; Shin, W.-C.; Lim, K.-T. Stimuli-responsive self-assembly of cellulose nanocrystals (CNCs): Structures, functions, and biomedical applications. *Int. J. Biol. Macromol.* **2020**, *155*, 456−469.
(21) Christau, S.; Moeller, T.; Genzer, J.; Koehler, R.; von Klitzing, R. Salt-induced aggregation of negatively charged gold nanoparticles confined in a polymer brush matrix. *Macromolecules* **2017**, *50*, 7333−7343.
(22) Wu, Y.-Y.; Huang, P.; Wu, F.-Y. A label-free colorimetric aptasensor based on controllable aggregation of AuNPs for the detection of multiplex antibiotics. *Food Chem.* **2020**, *304*, 125377.
(23) Fuller, M.; Köper, I. Polyelectrolyte-coated gold nanoparticles: the effect of salt and polyelectrolyte concentration on colloidal stability. *Polymers* **2018**, *10*, 1336.
(24) Carl, N.; Prévost, S.; Fitzgerald, J. P. S.; Karg, M. Salt-induced cluster formation of gold nanoparticles followed by stopped-flow SAXS, DLS and extinction spectroscopy. *Phys. Chem. Chem. Phys.* **2017**, *19*, 16348−16357.
(25) Hoeng, F.; Denneulin, A.; Neuman, C.; Bras, J. Charge density modification of carboxylated cellulose nanocrystals for stable silver nanoparticles suspension preparation. *J. Nanopart. Res.* **2015**, *17*, 244.
(26) Li, H.; Rothberg, L. Colorimetric detection of DNA sequences based on electrostatic interactions with unmodified gold nanoparticles. *Proc. Natl. Acad. Sci. U. S. A.* **2004**, *101*, 14036−14039.
(27) Budhadev, D.; Poole, E.; Nehlmeier, I.; Liu, Y.; Hooper, J.; Kalverda, E.; Akshath, U. S.; Hondow, N.; Turnbull, W. B.; Pöhlmann, S.; Guo, Y.; Zhou, D. Glycan-Gold Nanoparticles as Multifunctional Probes for Multivalent Lectin−Carbohydrate Binding: Implications for Blocking Virus Infection and Nanoparticle Assembly. *J. Am. Chem. Soc.* **2020**, *142*, 18022−18034.
(28) Bosak, A.; Saraf, N.; Willenberg, A.; Kwan, M. W. C.; Alto, B. W.; Jackson, G. W.; Batchelor, R. H.; Nguyen-Huu, T. D.; Sankarapani, V.; Parks, G. D.; Seal, S.; Willenberg, B. J. Aptamer−gold nanoparticle conjugates for the colorimetric detection of arboviruses and vector mosquito species. *RSC Adv.* **2019**, *9*, 23752−23763.
(29) Springer, V.; Segundo, M. A.; Centurión, M. E.; Avena, M. Fully-programmable synthesis of sucrose-mediated gold nanoparticles for detection of ciprofloxacin. *Mater. Chem. Phys.* **2019**, *238*, 121917.
(30) Sha, Q.; Guan, R.; Su, H.; Zhang, L.; Liu, B.-F.; Hu, Z.; Liu, X. Carbohydrate-protein template synthesized high mannose loading gold nanoclusters: A powerful fluorescence probe for sensitive Concanavalin A detection and specific breast cancer cell imaging. *Talanta* **2020**, *218*, 121130.
(31) Yrad, F. M.; Castañares, J. M.; Alocilja, E. C. Visual detection of dengue-1 RNA using gold nanoparticle-based lateral flow biosensor. *Diagnostics* **2019**, *9*, 74.
(32) Tammam, S. N.; Khalil, M. A. F.; Gawad, E. A.; Althani, A.; Zaghloul, H.; Azzazy, H. M. E. Chitosan gold nanoparticles for detection of amplified nucleic acids isolated from sputum. *Carbohydr. Polym.* **2017**, *164*, 57−63.
(33) Rezaei, Z. B.; Rastegarzadeh, S.; Kiasat, A. A Sensitive and Selective Colorimetric Probe for Cimetidine Determination Based on Surface Plasmon Resonance of Chitosan-Encapsulated Gold Nanoparticles. *Plasmonics* **2019**, *14*, 1169−1177.
(34) Bartosewicz, B.; Bujno, K.; Liszewska, M.; Budner, B.; Bazarnik, P.; Płociński, T.; Jankiewicz, B. J. Effect of citrate substitution by various α-hydroxycarboxylate anions on properties of gold nanoparticles synthesized by Turkevich method. *Colloids Surf., A* **2018**, *549*, 25−33.

https://doi.org/10.1021/acsomega.1c00359
ACS Omega 2021, 6, 12424−12431